

Observation of genuine three-photon interference

Sascha Agne*,¹ Thomas Kauten,² Jeongwan Jin,¹ Evan Meyer-Scott,^{1,3} Jeff Z. Salvail,¹
Deny R. Hamel,⁴ Kevin J. Resch,¹ Gregor Weihs,^{2,5} and Thomas Jennewein^{1,5}

¹*Institute for Quantum Computing and Department of Physics and Astronomy,
University of Waterloo, N2L 3G1, Ontario, Canada**

²*Institut für Experimentalphysik, Universität Innsbruck, Technikerstraße 25, 6020 Innsbruck, Austria*

³*Department of Physics, University of Paderborn,
Warburger Straße 100, 33098 Paderborn, Germany*

⁴*Département de Physique et d'Astronomie, Université de Moncton, Moncton, New Brunswick E1A 3E9, Canada*

⁵*Quantum Information Science Program, Canadian Institute for Advanced Research, Toronto, Ontario, Canada*

Multiparticle quantum interference is critical for our understanding and exploitation of quantum information, and for fundamental tests of quantum mechanics [1]. A remarkable example of multi-partite correlations is exhibited by the Greenberger-Horne-Zeilinger (GHZ) state [2]. In a GHZ state, three particles are correlated while no pairwise correlation is found [3]. The manifestation of these strong correlations in an interferometric setting has been studied theoretically since 1990 [2, 4–6] but no three-photon GHZ interferometer has been realized experimentally. Here we demonstrate three-photon interference that does not originate from two-photon or single photon interference. We observe phase-dependent variation of three-photon coincidences with $(90.5 \pm 5.0)\%$ visibility in a generalized Franson interferometer [7] using energy-time entangled photon triplets [8]. The demonstration of these strong correlations in an interferometric setting provides new avenues for multiphoton interferometry, fundamental tests of quantum mechanics and quantum information applications in higher dimensions.

In 1989, Franson [7] considered a light source that emits two photons simultaneously but at an unknown absolute time. These photon pairs, when sent through identical, but independent, unbalanced interferometers, display interference in the two-fold coincidence rate, but not in the independent single detection rates [9]. This is the simplest manifestation of what we call genuine interference: certain multipartite entangled quantum states display correlations in the highest order while interference that cannot be explained by lower-order interference [1, 2]. The Franson interferometer is representative of a class of two-particle interferometers that convert continuous-variable entanglement into two-valued observables via the two output ports of an interferometer [10]. Accordingly, with three independent interferometers, three continuously entangled photons can show genuine interference as well. This is known as the GHZ interferometer [2, 4–6] and is shown schematically in Fig. 1 (a). However, multiphoton entanglement experiments

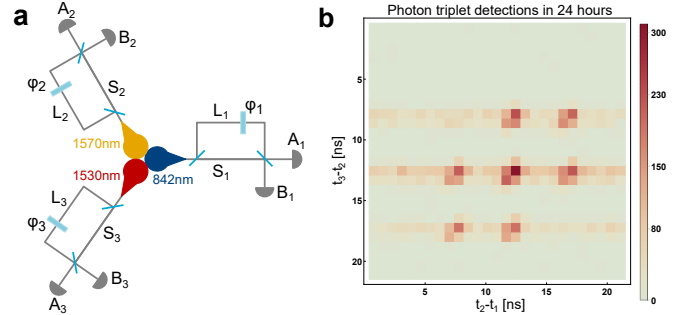


FIG. 1. **Three-photon Franson interferometer.** (a) Each of three energy-time entangled photons (at wavelengths 842, 1530 and 1570 nm) travels through an unbalanced interferometer with a path difference τ between the short (S) and long (L) paths. (b) The measured arrival time difference histogram with a bin size of 0.78 ns and peak separation of $\tau = 3.7$ ns displays seven narrow peaks corresponding to the eight possible path combinations $S_1S_2S_3$, $L_1S_2S_3$, $S_1L_2S_3$, $S_1S_2L_3$, $L_1L_2S_3$, $L_1S_2L_3$, $S_1L_2L_3$, and $L_1L_2L_3$. When all three photons take either the short or the long path the relative arrival time is the same, so the $S_1S_2S_3$ and $L_1L_2L_3$ events overlap, forming the central peak. This overlap is a coherent superposition, leading to a three-photon coincidence rate that depends on the phases φ_n ($n = 1, 2, 3$).

are considered less challenging when using polarization [11] and only Mermin’s “three-spin gadget” [12] has been realized [13] rather than the three-photon GHZ interferometer. Such an interferometer differs from previously realized NOON-type interferometers, where the photons are manipulated together in a single interferometer to show superresolution effects with, in general, non-zero lower-order interference [1, 6, 14, 15].

Energy-time entangled photon triplets can be described by a continuous superposition of triplet creation times [6],

$$|\Psi\rangle_{\text{Triplet}} = \int dt a_1^\dagger(t) a_2^\dagger(t) a_3^\dagger(t) |0\rangle. \quad (1)$$

We let each photon individually propagate through an unbalanced interferometer with a time difference $\tau = 3.7$ ns between short and long arm, as shown in Fig. 1a. The creation operators in equation (1) can be expressed

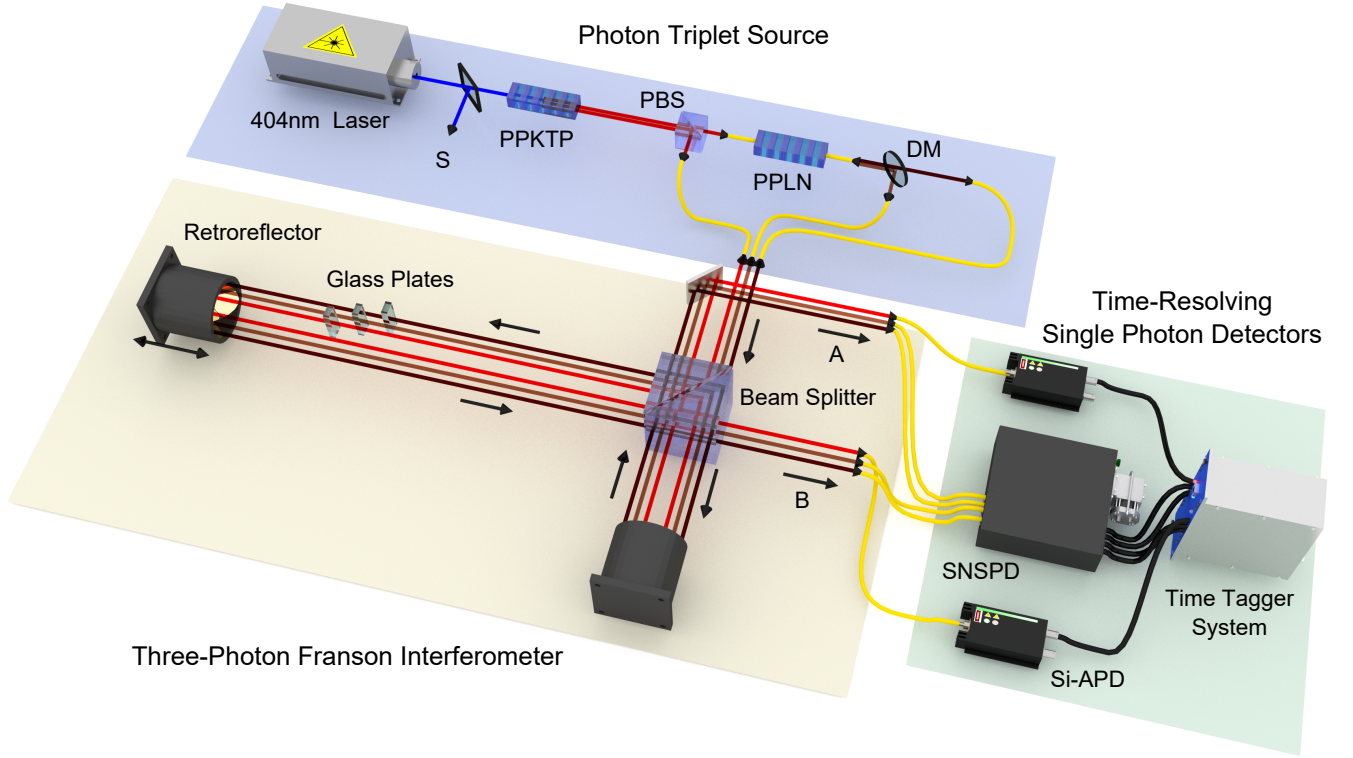


FIG. 2. **Experimental setup for the observation of genuine three-photon interference.** A continuous-wave grating-stabilized laser diode (404 nm, 43 mW, > 25 m coherence length) pumps a 25 mm periodically-poled potassium titanyl phosphate (PPKTP) crystal to generate pairs of 842/776 nm photons in type-II down-conversion, which are split at a polarizing beam splitter (PBS). The 776 nm photons pump a periodically-poled lithium niobate (PPLN) waveguide to generate 1530/1570 nm photon pairs in type-0 down-conversion. These infrared photons are split in free-space by a dichroic mirror (DM) before entering the three-photon Franson interferometer, which is realized as three spatial modes of a single interferometer with a path difference $\tau = 3.7$ ns. Photon phase control is achieved with motorized glass plates. At the two output ports A and B, the 842 nm and 1530/1570 nm photons are detected with free-running silicon avalanche photodiodes (Si-APD) and superconducting nanowire single photon detectors (SNSPD), respectively, and their arrival time is registered with a time tagger system. All fibers (yellow) are single-mode fibers at respective wavelengths. A few pump photons are picked off and sent through another interferometer path (S — not drawn) for interferometer stabilization, as explained in the Methods.

in terms of the detection modes A_n and B_n ($n = 1, 2, 3$) as

$$a_n^\dagger(t) = \frac{1}{2} \left[A_n^\dagger(t) + iB_n^\dagger(t) \right] - \frac{e^{i\varphi_n}}{2} \left[A_n^\dagger(t + \tau) + iB_n^\dagger(t + \tau) \right]. \quad (2)$$

The detection modes correspond to the complementary interferometer output modes and thus partition the eight possible detector combinations into even/odd parity sets

$$\begin{aligned} \text{AAA} &= \{A_1A_2A_3, A_1B_2B_3, B_1A_2B_3, B_1B_2A_3\} \\ \text{BBB} &= \{B_1B_2B_3, B_1A_2A_3, A_1B_2A_3, A_1A_2B_3\} \end{aligned} \quad (3)$$

Using detectors with ~ 1 ns time resolution, sufficiently shorter than the interferometer path difference, we can detect three photons simultaneously, selecting, for exam-

ple for $A_1A_2A_3$ coincidences, the output state [6]

$$|\Psi\rangle_{A_1A_2A_3} \propto \left[1 - \exp\left(i \sum_{n=1}^3 \varphi_n\right) \right] \int dt \prod_{n=1}^3 A_n^\dagger(t) |0\rangle. \quad (4)$$

From these we obtain the three-photon coincidence probabilities for the AAA (−) and BBB (+) combinations

$$P_3 = \frac{1}{2} [1 \pm \cos(\varphi_1 + \varphi_2 + \varphi_3)]. \quad (5)$$

Thus, the three-photon coincidence rate depends on the sum of the interferometer phases. Calculating the marginal probabilities, one can also show that the single photon and two-photon coincidence rates are constant [5].

The main experimental challenge in observing higher-order interference is posed by the low generation efficiency of multi-partite entangled states. The count rate in our experiment is critical since losses in the interferometers scale with the number of photons and only

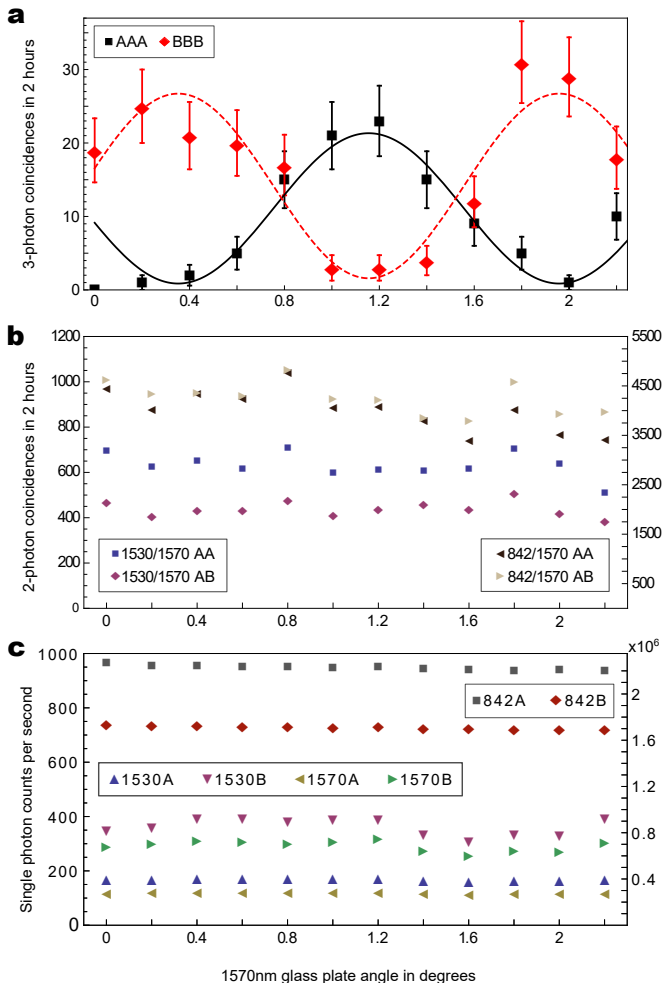


FIG. 3. Three-photon coincidences, two-photon coincidences and single photon counts in our three-photon Franson interferometer. The measured three-photon coincidences (a) show clear signature of interference with an average visibility of $(90.5 \pm 5.0)\%$ without background subtraction. The error bars are approximated by Poissonian count errors. No systematic modulation is visible in the measured (b) two-photon coincidences that can lead to a triplet in the histogram Fig. 1 (b) and (c) single detection rates. The letters in the legend of the two-fold coincidences indicate the set of detector combinations. For example 1530/1570 AA is the sum of 1530/1570 coincidences in detector combinations A_2A_3 and B_2B_3 .

one-quarter of the transmitted photon triplets contribute to the interference term, as is evident from Fig. 1 (b). Among the alternatives for the direct generation of photon triplets are $\chi^{(3)}$ -interaction in optical fibers [16], sum-frequency generation of energy-time entangled photon pairs [17] and cascaded spontaneous parametric down-conversion (CSPDC) [8]. We employ a newly designed CSPDC source that produces photon triplets at a high rate in a state that approximates the triplet state in equation (1) (see Methods). The full experimental setup that we use to achieve sufficiently low losses to compile robust

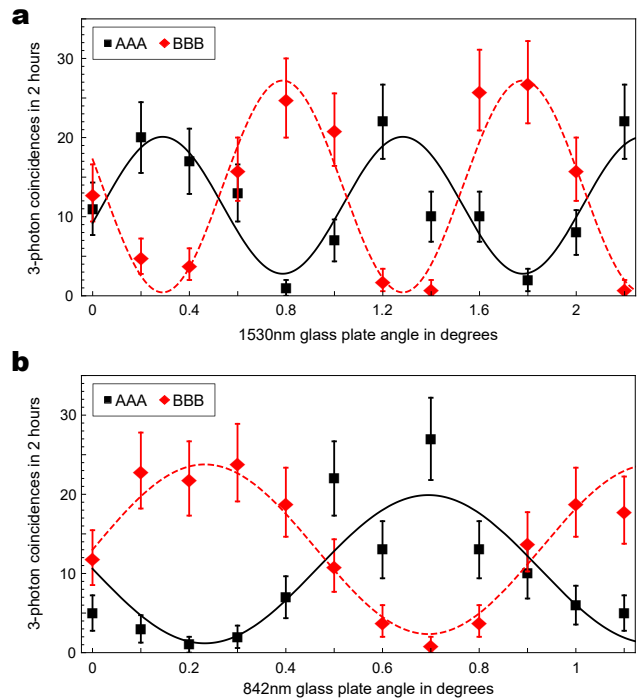


FIG. 4. Further evidence for genuine three-photon interference. The phase scan for 1530 nm (a) and 842 nm (b) photons of photon triplets yield average interference visibilities of $(86.1 \pm 5.3)\%$ and $(85.4 \pm 5.7)\%$, respectively. As for the 1570 nm phase scan, the two-photon coincidences and single detection rates show no modulation.

measurement statistics is shown in Fig. 2 with additional details available in the Methods.

We first record photon events for 12 phase settings of the 1570 nm photons by changing the angles of the glass phase plate in the 1570 nm long arm. Measuring for 2 hours per angle, over 24 hours we detect 4648 triplets within a coarse 20 ns coincidence window. The histogram in Fig. 1 (b) shows the distribution of arrival times with seven peaks that reflect the eight possible path combinations. With a bin size of 0.78 ns in both dimensions, we have 309 triplets in the central bin and an average of 137 triplets in each of the six highest side bins. The triplets in the central bin are shown as a function of the 1570 nm glass phase plate angle in Fig. 3 (a) and fits of equation (5) yield visibilities $V_{AAA} = (92.2 \pm 6.3)\%$ and $V_{BBB} = (88.8 \pm 7.9)\%$. This gives an average visibility of $(90.5 \pm 5.0)\%$ without background subtraction (see Methods), which is above the classical visibility bound of 50% for genuine three-photon interference [18, 19].

As shown in Fig. 3 (b) and (c), the two-photon coincidences and single count rates from the same data set display only small drifts in count rates over the course of the experiment but no systematic, complementary modulation. Variations in the two-photon coincidences can be due to fluctuations in the mean SNSPD dark count rate, which affects the observed three-fold coincidences.

For example, comparing Fig. 3 (a) and (b) at angles 0.8 and 1.6 we see that the higher three-fold coincidences agree with an isolated increase in two-fold coincidences. Note that whereas the infrared singles are dominated by dark counts, the ratio of signal to dark counts per second in the Si-APDs is $\sim 10^5$ and therefore any modulation present in the 842 nm single counts would be clearly visible.

In a second measurement, we scan the phase of 1530 nm photons. Fig. 4 (a) shows the result of a scan in which the 1530 nm glass phase plate is pre-tilted (see Methods) so that two fringes are observed over 2.2 degrees. The three-photon interference average visibility is $(86.1 \pm 5.3)\%$ ($V_{AAA} = (75.6 \pm 9.5)\%$ and $V_{BBB} = (96.9 \pm 4.6)\%$) without background subtraction. The phase of 842 nm photons is scanned in a third measurement. Given that the wavelength is about half the other photon's wavelengths and the glass plates have identical thicknesses, we expect a full three-photon interference fringe over half the 1570 nm scan range. Indeed, as Fig. 4 (b) shows, we observe a fringe with $(85.4 \pm 5.7)\%$ average visibility ($V_{AAA} = (88.8 \pm 8.0)\%$ and $V_{BBB} = (82.0 \pm 8.3)\%$) without background subtraction. In a last series of measurements, we block individual or all interferometer paths and record photon events. The result figures can be found in the Supplementary Information. The three-photon coincidences show no phase dependence, demonstrating that the modulation with all interferometer paths open is due to interference.

We have experimentally shown that genuine three-photon interference is accessible with energy-time entangled photon triplets. Such states and the new quantum interference phenomena they exhibit suggest several interesting directions for future research. Using a pulsed pump, our experimental apparatus should be able to generate and analyze three-photon time-bin states [20] for direct implementations of quantum communication protocols [21]. Our setup could be converted to perform NOON-style interferometry with applications in phase superresolution and supersensitivity [6]. Furthermore, this system could be used for fundamental questions of non-locality [22] in tests of both Mermin [23] and Svetlichny inequalities [24], more detailed study on the three-photon joint-spectral function [25], and enable the realization and study of genuine tripartite hyperentanglement [26].

* sascha.agne@uwaterloo.ca

- [1] Pan, J. W. et al. Multiphoton entanglement and interferometry. *Rev. Mod. Phys.* **84**, 777 (2012).
- [2] Greenberger, D. M., Horne, M. A., Shimony, A. & Zeilinger, A. Bell's theorem without inequalities. *Am. J. Phys.* **58**, 1131 (1990).
- [3] Bouwmeester, D., Pan, J.-W., Daniell, M., Weinfurter, H. & Zeilinger, A. Observation of three-photon greenberger-horne-zeilinger entanglement. *Phys. Rev. Lett.* **82**, 1345 (1999).
- [4] Greenberger, D. M., Horne, M. A. & Zeilinger, A. Multiparticle interferometry and the superposition principle. *Physics Today* **46**, 22 (1993).
- [5] Rice, D. A., Osborne, C. F. & Lloyd, P. Multiparticle interference. *Phys. Lett. A* **186**, 21 (1994).
- [6] Barnett, S. M., Imoto, N. & Huttner, B. Photonic de Broglie wave interferometers. *J. Mod. Opt.* **45**, 2217 (1998).
- [7] Francon, J. D. Bell inequality for position and time. *Phys. Rev. Lett.* **62**, 2205 (1989).
- [8] Hübel, H. et al. Direct generation of photon triplets using cascaded photon-pair sources. *Nature* **466**, 601 (2010).
- [9] Kwiat, P. G., Steinberg, A. M. & Chiao, R. Y. High-visibility interference in a Bell-inequality experiment for energy and time. *Phys. Rev. A* **47**, 2472 (1993).
- [10] Horne, M. A., Shimony, A. & Zeilinger, A. Two-particle interferometry. *Phys. Rev. Lett.* **62**, 2209 (1989).
- [11] Zeilinger, A., Horne, M. A., Weinfurter, H. & Żukowski, M. Three-particle entanglements from two entangled pairs. *Phys. Rev. Lett.* **78**, 3031 (1997).
- [12] Mermin, N. D. Quantum mysteries revisited. *American Journal of Physics* **58**, 731 (1990).
- [13] Pan, J.-W., Bouwmeester, D., Daniell, M., Weinfurter, H. & Zeilinger, A. Experimental test of quantum nonlocality in three-photon greenberger-horne-zeilinger entanglement. *Nature* **403**, 515 (2000).
- [14] Walther, P. et al. De Broglie wavelength of a non-local four-photon state. *Nature* **429**, 158 (2004).
- [15] Mitchell, M. W., Lundeen, J. S. & Steinberg, A. M. Super-resolving phase measurements with a multiphoton entangled state. *Nature* **429**, 161 (2004).
- [16] Corona, M., Garay-Palmett, K. & U'Ren, A. B. Experimental proposal for the generation of entangled photon triplets by third-order spontaneous parametric downconversion in optical fibers. *Optics Letters* **36**, 190 (2014).
- [17] Guerreiro, T. et al. Nonlinear interaction between single photons. *Physical Review Letters* **113**, 1–5 (2014).
- [18] Klyshko, D. N. The Bell and GHZ theorems: a possible three-photon interference experiment and the question of nonlocality. *Phys. Lett. A* **172**, 399 (1993).
- [19] Belinsky, A. V. & Klyshko, D. N. A modified N-particle Bell theorem, the corresponding optical experiment and its classical model. *Phys. Lett. A* **176**, 415 (1993).
- [20] Brendel, J., Gisin, N., Tittel, W. & Zbinden, H. Pulsed energy-time entangled twin-photon source for quantum communication. *Phys. Rev. Lett.* **82**, 2594 (1999).
- [21] Hillery, M., Bužek, V. & Berthiaume, A. Quantum secret sharing. *Phys. Rev. A* **59**, 1829 (1999).
- [22] Vallone, G., Mataloni, P. & Cabello, A. Multiparty multilevel energy-time entanglement. *Phys. Rev. A* **81**, 032105 (2010).
- [23] Mermin, N. D. Extreme quantum entanglement in a superposition of macroscopically distinct states. *Phys. Rev. Lett.* **65**, 1838 (1990).
- [24] Svetlichny, G. Distinguishing three-body from two-body nonseparability by a Bell-type inequality. *Phys. Rev. D* **35**, 3066 (1987).
- [25] Shalm, L. K. et al. Three-photon energy-time entanglement. *Nat. Phys.* **9**, 19 (2012).
- [26] Barreiro, J. T., Langford, N. K., Peters, N. A. &

Kwiat, P. G. Generation of hyperentangled photon pairs. *Phys. Rev. Lett.* **95**, 260501 (2005).

[27] Hamel, D. R. et al. Direct generation of three-photon polarization entanglement. *Nat. Phot.* **8**, 801 (2014).

ACKNOWLEDGMENT

We gratefully acknowledge supports through the Canadian Institute for Advanced Research (CIFAR), the Canada Foundation for Innovation (CFI), the Office of Naval Research (ONR), the New Brunswick Innovation Foundation (NBIF), the Natural Sciences and Engineering Research Council of Canada (NSERC), the Ontario Research Fund (ORF), Canada Research Chairs, Industry Canada, the Korea Institute of Science and Technology (KIST) and the European Research Council (ERC) through project 257531 - EnSeNa. Furthermore, we like to thank Aaron Miller from Quantum Opus for providing and optimizing the superconducting nanowire single photon detectors.

AUTHOR CONTRIBUTIONS

S.A., T.K. and J.J. carried out the experiment with help from J.Z.S. and E.M.-S. All authors discussed the results and S.A., D.H., T.K. and T.J. analyzed the data. T.J. conceived the experimental idea and T.J., G.W., K.J.R., D.H., T.K., E. M.-S. and S.A. developed the experimental setup. T.K. build the interferometer and S.A. wrote the manuscript with contributions from all authors.

METHODS

Wavefunction approximation

The state produced in CSPDC is given by [25]

$$|\Psi\rangle_{\text{CSPDC}} \approx \int_{\omega_1} \int_{\omega_2} d\omega_1 d\omega_2 G_1(\omega_1, \omega_p - \omega_1) G_2(\omega_2, \omega_p - \omega_1 - \omega_2) a_1^\dagger(\omega_1) a_2^\dagger(\omega_2) a_3^\dagger(\omega_p - \omega_2 - \omega_1) |0\rangle$$

with the two joint-spectral functions G_1 and G_2 determined by phase-matching conditions. We obtain equation (1) by approximating G_1 and G_2 with a constant and performing a Fourier transform. This infinite-bandwidth approximation is supported by the broad single photon spectra (see Fig. 1 and 2 in the Supplementary Information).

Experimental Design

We improved on previous CSPDC sources [8, 25, 27] with a brighter first-stage pair source (we detect 3.8 million 776/842 nm pairs per second). The spectra of the triplet photons can be found in the Supplementary Information. To avoid the cross-stabilization of three spatially separated interferometers we combine the interferometers to use a common beam splitter and retroreflectors, with four well-separated paths for 842 nm, 1530 nm, 1570 nm and 404 nm photons. The 404 nm photons are obtained from the pump laser and are used to stabilize the interferometer via a piezo electric actuator attached to the long-arm retroreflector in a feedback loop. The monolithic design allows us to perform phase-stable experiments over at least 96 hours and gives us more than 44% transmission for all paths, including fiber coupling losses. The phases of the 842 nm, 1530 nm and 1570 nm photons are individually controlled via motorized glass phase plates (BK7 windows with a thicknesses of 3 mm and anti-reflection coated at the respective wavelength) in the long arm. We characterize the zero-position of the glass phase plates with lasers and verify the nonlinear relationship between glass phase plate angle and induced phase. Based on these measurements, we pre-tilt the glass phase plate by a few degrees to observe at least one fringe over two degrees and define the pre-tilt angle as the zero-position for our measurements. For the detection of the infrared photons, we employ four SNSPDs with efficiencies 80, 48, 60 and 85 % and 150-400 dark counts per second. The time tagger system assigns time stamps to single photon detection events with 78 ps resolution, whereby we obtain information about single photon detections as well as two-photon and three-photon coincidences during data analysis.

Visibility Estimation

To estimate the fringe visibility, we fit $f(x) = a_1[1 + V_1 \sin(b_1 \cdot x + c_1)]$ to the AAA data and then use b_1 and c_1 for fitting $g(x) = a_2[1 + V_2 \sin(b_1 \cdot x + c_1)]$ to the BBB data. From the original data set, ten new data sets are generated from a Poisson distribution with mean equal to the measured data points. Following the same fitting procedure as above, the visibility was obtained for each sample. The standard deviation of these visibilities form the visibility error bound.

SUPPLEMENTARY INFORMATION

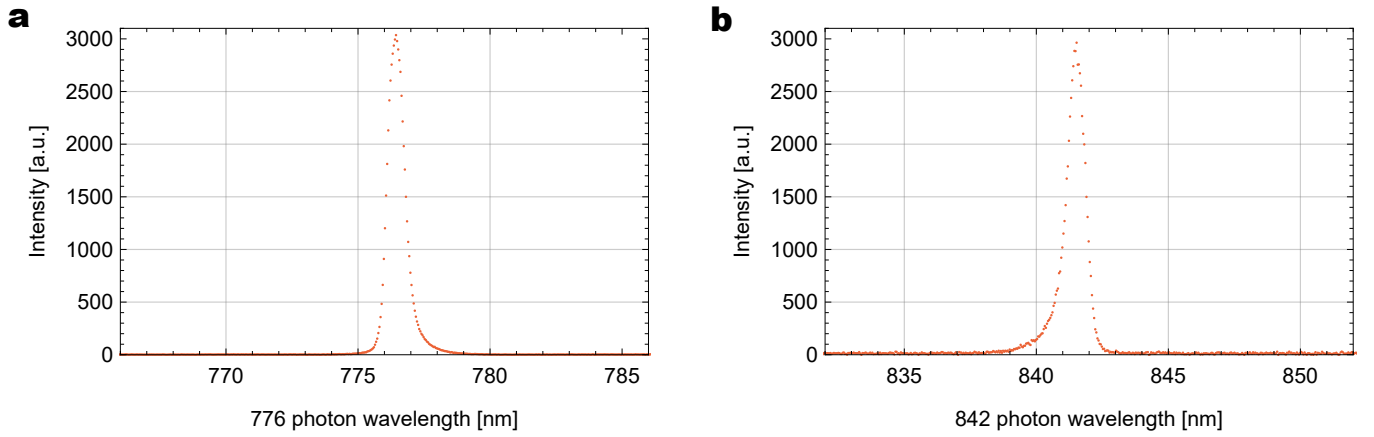


FIG. 5. **Spectra of the two near-infrared photons used in the experiment.** We fit Gaussian functions $I(x) = I_0 \exp(-(\lambda - \lambda_0)/2\sigma^2)$ to the peak and calculate the full width at half maximum $\text{FWHM} = 2\sqrt{2 \ln(2)}\sigma$: $\text{FWHM}_{776} = 0.75$ nm and $\text{FWHM}_{842} = 0.86$ nm. The center wavelengths are $\lambda_{0,776} = 776.45$ nm and $\lambda_{0,842} = 841.50$ nm. The finite width introduces a phase error $\Delta\phi = \Delta\lambda/\lambda \approx 0.1\%$

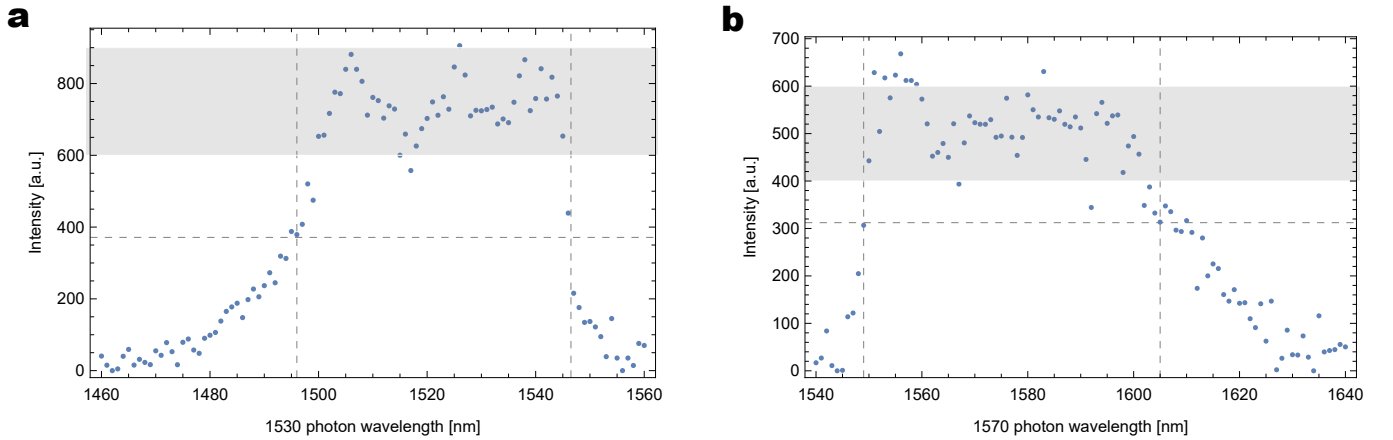


FIG. 6. **Spectra of the two infrared photons used in the experiment.** We measured these by pumping the PPLN waveguide with 776 nm light from a mode-locked Ti:sapphire laser (Coherent MIRA 900) whose spectrum approximates that of the 776 nm photons from the PPKTP, and scanning a diffractive spectrometer coupled to a single-photon detector. Here the pump bandwidth is of the same order as the acceptance band of the PPLN waveguides, leading to non-Gaussian output spectra by summing over many down-conversion spectral modes. We estimate the spectral width by the full width at half maximum (FWHM) of a moving average fit (solid line). We obtain $\text{FWHM}_{1530} = (51 \pm 1)$ nm and $\text{FWHM}_{1570} = (60 \pm 1)$ nm, respectively. The finite width introduces phase errors $\Delta\phi = \Delta\lambda/\lambda$, which is about 3% for both photons.

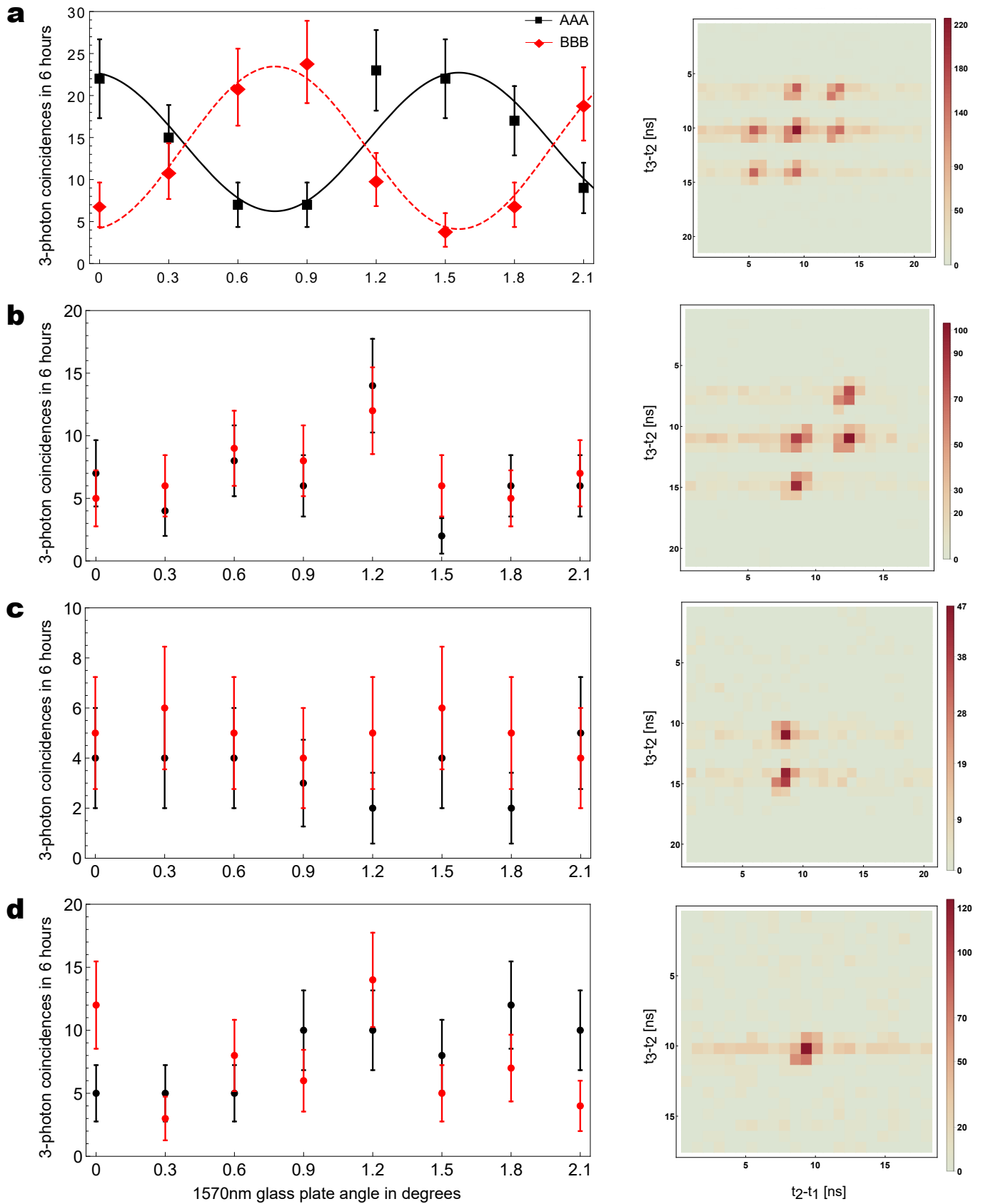


FIG. 7. **Blocked paths three-photon interference experiments.** These measurements compare the cases when all paths are open (a), the 842 nm long path is blocked (b), the 842 nm and 1530 nm long paths are blocked (c) and all short paths are blocked (d). The histograms reflect the restriction to path combinations $(S_1S_2S_3, S_1S_2L_3, S_1L_2S_3, S_1L_2S_3)$, $(S_1S_2S_3, S_1S_2L_3)$ and $L_1L_2L_3$, respectively. In each case, the AAA and BBB detector combinations show no complementary coincidences. Note that the count rates here are much lower than for the measurements reported in the main text and only eight phase settings were used. The reason is that these measurements were carried out in the beginning where we used SNSPDs with lower efficiencies and higher dark counts.